Eur. Phys. J. B **42**, 193–204 (2004)
DOI: 10.1140/epjb/e2004-00372-9

THE EUROPEAN PHYSICAL JOURNAL B

Magnetic texturing of xenon-ion irradiated nickel films

K. Zhang[1], K.P. Lieb[1,a], G.A. Müller[1], P. Schaaf[1], M. Uhrmacher[1], and M. Münzenberg[2]

[1] II. Physikalisches Institut and Sonderforschungsbereich 602, Universität Göttingen, Friedrich-Hund-Platz 1, 37077 Göttingen, Germany
[2] IV. Physikalisches Institut, Universität Göttingen, Friedrich-Hund-Platz 1, 37077 Göttingen, Germany

Received 29 July 2004 / Received in final form 30 September 2004
Published online 14 December 2004 –

Abstract. Thin polycrystalline Ni films of typically 75 nm thickness evaporated on Si or SiO_2 substrates were irradiated with 30–900 keV Xe-ions to fluences of $2.5\times10^{13}-4\times10^{14}/\mathrm{cm}^2$. The magnetization of the Ni films was measured using the longitudinal Magneto-Optical Kerr Effect and Vibrating Sample Magnetometry. The Ni-film thickness and Xe-concentration profiles were determined with Rutherford backscattering spectroscopy and the lattice dilation with X-ray diffraction. The Xe-irradiations were found to induce an in-plane uniaxial magnetic anisotropy within the Ni-films. This magnetic texture was investigated in relationship to the microstructure as function of the ion energy and fluence, the sample temperature, the presence of an external magnetic field during the irradiation and the stress field produced before, during and after the implantations.

PACS. 61.82.Bg Metals and alloys – 68.55.Ln Defects and impurities: doping, implantation, distribution, concentration, etc. – 75.30.Gw Magnetic anisotropy – 75.70.-i Magnetic properties of thin films, surfaces, and interfaces

1 Introduction

For decades, induced magnetic anisotropies in ferromagnetic nanometer films have been an exciting field [1,2]. The magnetic and structural properties of such films are known to be influenced by the conditions prevailing during the production or treatment of the films. In-plane magnetic anisotropies may be induced during deposition in a magnetic or electric field [3,4], as a result of thermal or ion-beam assisted deposition [5,6] and during sputtering onto bent substrates [7]. In the case of Ni-films, the magnitude and spatial orientation of the magnetic moments may also depend on parameters such as film thickness, type of substrate, interface structure or a possible buffer layer, and other preparation conditions, such as the temperature of the substrate and the magnetic field applied either during film deposition or subsequent annealing.

Ion beam irradiation of thin ferromagnetic films or multilayers offers another and possibly technologically interesting means of changing their magnetic properties. As examples, here we only mention the results obtained by Lewis et al. [6] and by Farle et al. [8] for Ni- and Fe-films produced with noble-gas ion-beam-assisted deposition, and the extensive findings of the Orsay group after He-irradiation of Pt/Co/Pt multilayers [9–11]. On the basis of Perturbed Angular Correlation (PAC) experiments with dilute ^{111}In tracers, Wodniecki et al. [12] and Neubauer et al. [13,14] demonstrated that heavy-ion irradiated polycrystalline Fe- and Ni-films show dramatic changes of their magnetic properties. Noble-gas ion irradiations with fluences as low as some $10^{14}/\mathrm{cm}^2$ were found to change the originally isotropic distribution of the magnetization into a uniaxially oriented magnetization within the film plane, called magnetic texture. Recent Magnetical Orientation Electron Moessbauer (MOMS) analyses confirmed this result for Xe-irradiated Fe films [15]. Finally, Xe-ion irradiated Co-films or Co/Fe-bilayers exhibit pronounced phase transitions as demonstrated by Zhang and collaborators on the basis of magnetic anisotropy measurements [16–18].

The motivation for the present work was firstly to carry out a systematic study of this magnetic texturing effect in polycrystalline Ni-films by using the Magneto-Optical Kerr Effect (MOKE) and Vibrating Sample Magnetometry (VSM). Secondly, we wanted to vary, in a defined way, some of the essential parameters such as the external magnetic field or temperature during implantation as well as the internal, ion-induced and external stresses. Finally, we attempted to correlate the ion-induced changes of magnetic properties with the changes of the microstructure as determined with X-ray diffraction (XRD). A few preliminary results have been reported in [19,20].

[a] e-mail: plieb@gwdg.de

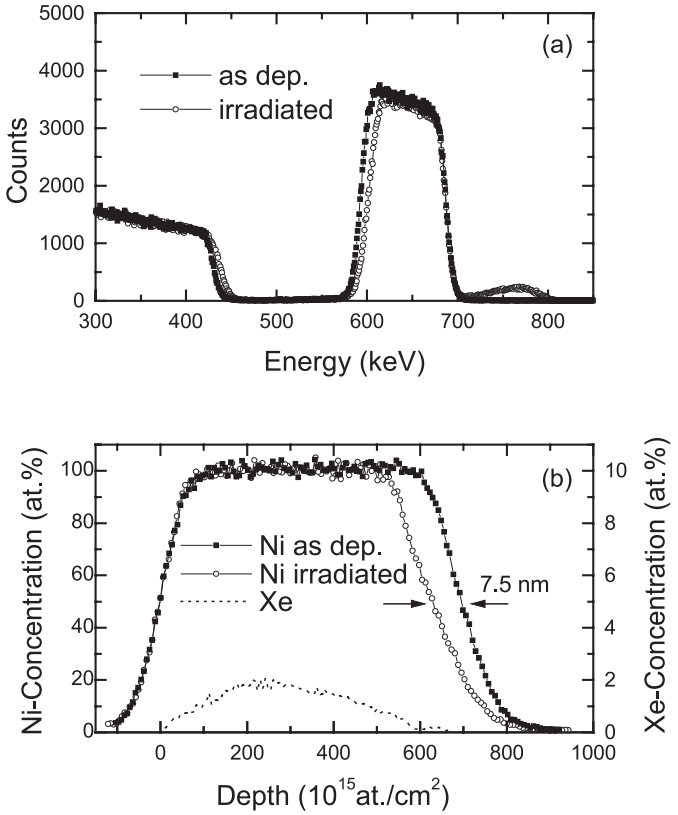

Fig. 1. RBS-spectra (a) and concentration profiles (b) of a Ni/Si-sample, as-deposited and after Xe-ion irradiation at the (very high) fluence of 1×10^{16}/cm^2. Note the 7.5 nm decrease in film thickness and the surface roughening due to sputtering and the accumulation of xenon within the Ni-film.

2 Experimental details

Using electron-gun evaporation, the 50–120 nm Ni films were deposited onto Si(100), Si(111) or amorphous SiO_2 substrates, which were mounted at a distance of 26 cm from the electron gun. During the deposition at a rate of 0.1 nm/s, the substrates were not cooled. The magnetic field during deposition was 0.82 Oe, having a 0.62 Oe component along the film plane. In general, the Ni films had a thickness of 75 nm and were rectangular in shape (10×7 mm^2). The pressure in the evaporation chamber was 2×10^{-6} mbar during deposition.

The Xe-ion implantations were carried out at the Göttingen ion accelerator IONAS [21] at a pressure of 5×10^{-7} mbar and at normal incidence. An electric xy-sweeping system of the ion beam was used in order to cover the implantation area homogeneously. The standard implantation energy was 200 keV. This choice implies an average ion range of 30 nm in Ni. Only a 0.1%-fraction of the implanted Xe ions thus penetrated the Ni/substrate interface and could induce ion mixing effects [22–26]. The implantations were performed at either liquid nitrogen or room temperature. Most samples were attached to Cu-target holders by silver paste without exerting any mechanical stress.

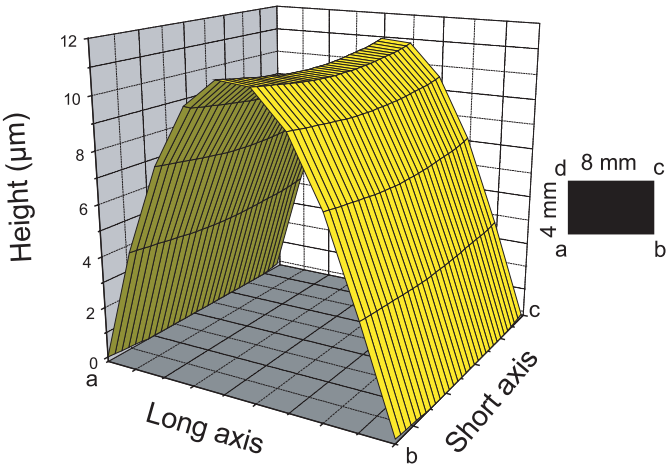

Fig. 2. Height profile of an 8×4 mm^2 Ni-film deposited onto a 40×15 mm^2 Si-wafer, which was bent to a curvature of $1/R = 1.9$ m^{-1}. The bending axis was the short axis of the sample.

All the as-deposited and ion-irradiated films underwent an RBS analysis using the 0.9 MeV α-particle beam of IONAS [21]. As an example, Figure 1 illustrates backscattering spectra and deduced Ni- and Xe-concentration profiles obtained for a 75 nm thick Ni/Si(100) bilayer, which was irradiated with the (unusually high) implantation fluence of 1×10^{16} Xe/cm^2. One notes the 7.5 nm sputtering effect, the increased surface roughness, visible as a smoother back-edge of the Ni profile, and the distribution of the implanted Xe content reaching a maximum of 2 at.%. The standard implantation fluences ranged from 2.5×10^{13} to 4×10^{14} Xe-ions/cm^2 and imply a maximum Xe-concentration of 0.1 at.% at the highest fluence.

XRD-analyses were performed in θ-2θ geometry using the Cu-K_α line and a Bruker AXS-D8 Advance spectrometer. The prominent Ni(111) diffraction peak indicated a strong (111) texture of all the Ni-films evaporated onto the Si(100), Si(111) and SiO_2 substrates.

In order to vary the external strain in some of the samples during or after ion implantation, 10×7 mm^2 Ni films were deposited in the center of 40×15 mm^2 Si(100)-wafers, which were bent along the short or long axis to curvatures of up to 2 m^{-1}. The radius R of the curvature was determined by measuring the surface profile by means of a Dektat^{3}ST profilometer, having a depth resolution of about 3 nm. A typical surface profile of a bent sample is illustrated in Figure 2.

The majority of magnetic analyses were carried out with the MOKE-technique using the longitudinal Kerr effect and a 2 mW HeNe laser with a diameter of 1.5 mm. Its sensitivity was 0.04°/mV [27–29]. The polarizing field H_{MOKE} of up to 900 Oe was generated by Helmholtz coils, but was not strong enough to saturate all the as-deposited samples. In all the MOKE-analyses, the in-plane angle of rotation, φ, of the external MOKE field refers to the

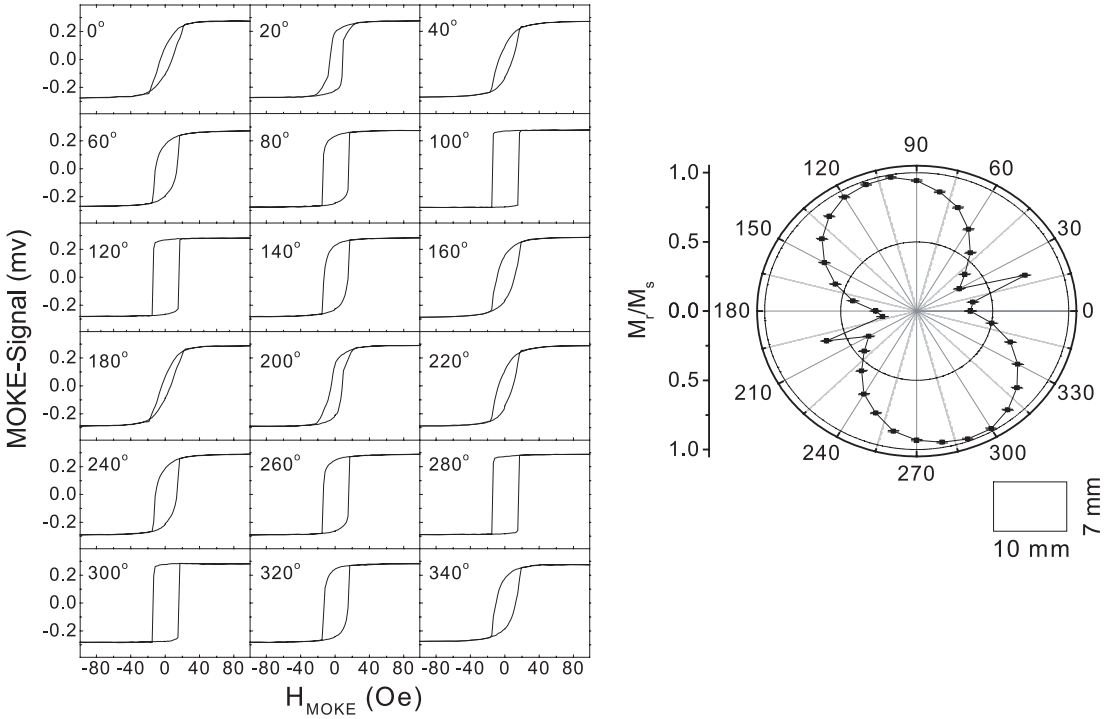

Fig. 3. Hysteresis curves (left) and polar diagram of the remanence parameter $R_e = M_r/M_s$ (right) of a 75 nm thick Ni/Si(100)-film of size 7×10 mm^2 irradiated with 4×10^{14} 200 keV Xe^+-ions/cm^2 at 100 K. The orientation of the external MOKE-field H_{MOKE} is relative to the long axis of the film ($\varphi = 0°$).

long axis of the sample. The magnetic parameters deduced from the MOKE analysis are the coercive field $H_c(\varphi)$, the remanence $M_r(\varphi)$, given either in arbitrary units or normalized to the corresponding saturation value $M_s(\varphi)$, $R_e(\varphi) \equiv M_r(\varphi)/M_s(\varphi)$, and the anisotropy field along the hard axis, $H_a = H_s - H_c$. For a quantitative measure of the magnetization and the changes induced during ion implantation, a 75 nm Ni-film in the as-deposited and irradiated state was also analyzed with VSM using an external field of up to 10 kOe.

3 Results

3.1 Ion-induced magnetic texturing of Ni films

Changes of the magnetization in Ni-films due to Xe-ion implantations, as seen with MOKE, are illustrated in Figure 3. Here we used a 75 nm Ni/Si(100)-sample irradiated at 100 K with 4×10^{14} ions/cm^2 at 200 keV. Figure 3 displays the hysteresis curves after irradiation measured in steps of 20° and, on the right-hand side, the deduced polar diagram of the relative remanence, $R_e(\varphi) \equiv M_r(\varphi)/M_s(\varphi)$. The easy magnetic axis is evidently at $\varphi \approx 120°$ and 300°, while the hard axis is around 30° and 210°. The relative remanence $R_e(\varphi)$ follows an angular dependence valid e.g. for magnetic stripe domains [30],

$$R_e(\varphi) = R_0 + R_D|\cos(\varphi - \varphi_0)|, \qquad (1)$$

with a small isotropic component of $R_0 = 0.06$. Deviations of the R_e-curves from this uniaxial dipolar pattern, in particular additional sharp peaks in the direction of the hard axis giving rise to a quadrupolar pattern, will not be discussed in this paper. Another important effect of the ion irradiation refers to a strong reduction and anisotropy of the coercive field H_C, from $H_C \approx 200-350$ Oe in the as-deposited state to $H_C \approx 10-20$ Oe in the easy axis, after the ion implantation.

These results were confirmed by a VSM-analysis of a 75 nm sample irradiated at room temperature with 4×10^{14} Xe-ions/cm^2, as can be seen in Figure 4. The in-plane coercive field was reduced from 200 Oe to 15 Oe. The in-plane and out-of-plane saturation magnetizations were found as $M_s = 473(5)$ emu/cm^3, in both the as-deposited and irradiated films. This value is close to that of Ni-bulk material at 300 K, $M_s = 485$ emu/cm^3 [31], and in 50–60 nm Ni-films [32]. Hence ion irradiation did not change the saturation magnetization, but the shape of the in-plane hysteresis curve.

3.2 Influence of substrate and size of irradiation and laser spot

In order to test the relevant parameters, which may influence the magnetic texturing effect, we first studied the influence of the substrate, on which the polycrystalline Ni-films were deposited. To this end we measured MOKE-patterns for 75 nm thick Ni-films deposited on Si(100),

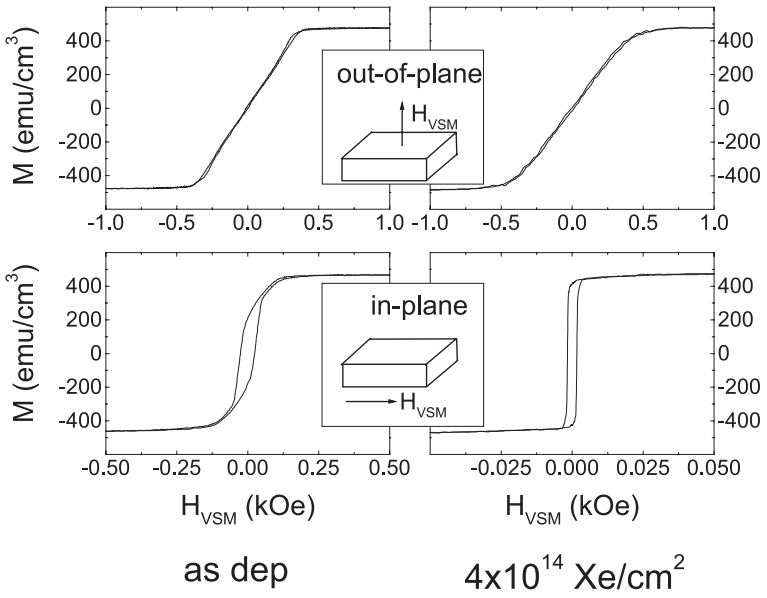

Fig. 4. VSM-hysteresis loops measured at room temperature before (a) and after (b) 200 keV Xe-ion irradiation of a 75 nm thick Ni/Si(100)-film with 4×10^{14} ions/cm^2 at 100 K.

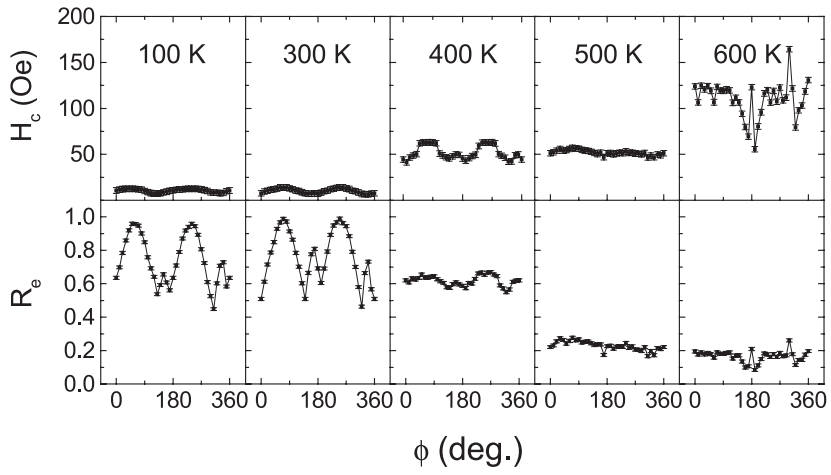

Fig. 5. Angular variations of the coercive field $H_C(\varphi)$ and the relative remanence $R_e(\varphi) = M_r(\varphi)/M_s(\varphi)$ for 75 nm Ni/Si-films irradiated with 200 keV Xe^+-ions to 4×10^{14}/cm^2 at different temperatures. The films had a circular form with a diameter of 8 mm. The direction $\varphi = 0^\circ$ refers to the horizontal line during the ion irradiations.

Si(111) or amorphous SiO_2 and irradiated with 200 keV Xe-ions at 100 K and a fluence of 4×10^{14} ions/cm^2. Before ion irradiation, all three films exhibited isotropic MOKE-patterns. After irradiation, they were strongly anisotropic and almost identical showing saturation of the magnetization at less than 100 Oe and a dramatic decrease of the coercivity: for both Ni/Si(100) and Ni/Si(111) samples, the values of $H_C(\varphi)$ ranged from 7 to 16 Oe in all the directions, those for the Ni/a-SiO_2 film from 5 to 22 Oe. In conclusion, the three substrates had almost no influence on the magnetic texturing of the Ni-films.

In order to investigate whether ion-irradiation over the full or partial sample surface area would change the magnetic texture, two 120 nm thick 10×10 mm^2 Ni/Si(100) films were irradiated with 450 keV Xe^+-ions at a fluence of 2×10^{14} ions/cm^2 each. In one sample the 5×5 mm^2 irradiation spot was centered by a mask, while the other sample was homogeneously irradiated over the full surface. MOKE-measurements were performed with a 1.5 mm and a 0.3 mm in-diameter laser beam both in the center and at the outer parts of the films. In both films, the angular modulations of $H_C(\varphi)$ and $R_e(\varphi)$ did not reveal any position sensitivity, while for the partially covered sample, the outer zone showed no magnetic anisotropy. These experiments were repeated for 18–160 nm thick Ni-films irradiated at energies to stop the ions in the middle of the Ni-layer, and again no significant dependence was found. We conclude that within the size of the ion-irradiated spot the magnetic texture is uniform.

3.3 Temperature dependence of the magnetic texture

In this series of measurements, the influence of the sample temperature during implantation was investigated by

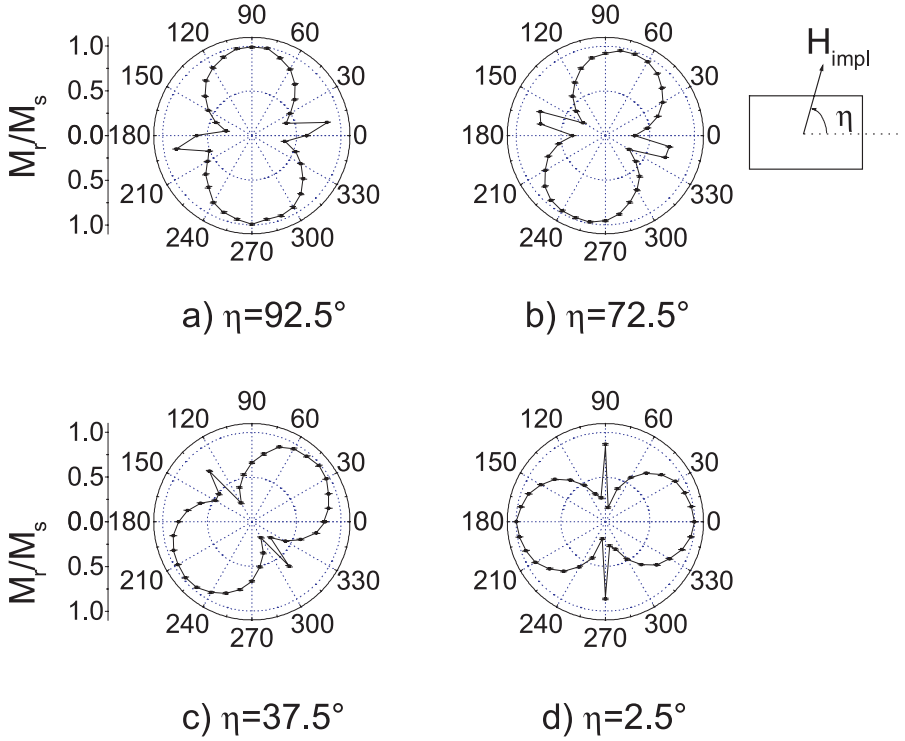

Fig. 6. MOKE-patterns obtained after irradiation 75 nm Ni films with 200 keV Xe-ions at a fluence of $4 \times 10^{14}/\mathrm{cm}^2$ under an external field of 104 Oe. The orientation of this field relative to the long axis of the samples is denoted by the angle η.

MOKE. Five 75 nm thick Ni/Si(100)-bilayers, of circular shape and 8 mm in diameter, were irradiated at 100, 300, 400, 500 and 600 K under standard implantation conditions (200 keV Xe^+-ions, $4 \times 10^{14}/\mathrm{cm}^2$). Figure 5 displays the angular dependence of the coercive field $H_C(\varphi)$ and relative remanence $R_e(\varphi)$. The angle $\varphi = 0°$ here refers here to the horizontal direction during implantation. For the as-deposited films we found a strong coercive field of $H_C \approx 350$ Oe and a nearly isotropic relative remanence of $R_e \approx 0.5$. Dramatic changes occurred in the films irradiated at 100 K and 300 K, which exhibited very similar hysteresis loops and angular modulations of $H_C(\varphi)$ and $R_e(\varphi)$. A magnetic field of 100 Oe was sufficient to saturate the magnetization of these two films and the mean values of $H_C(\varphi)$ decreased to 12(2) Oe.

The film irradiated at 400 K needed a saturation field of slightly above 900 Oe, which was the highest available field strength of the MOKE-apparatus used. For the irradiations at 500 and 600 K, the magnetization of the samples was not saturated. In these three cases, the relative remanence $R_e(\varphi)$ was defined as the ratio of the magnetization at $H_{\mathrm{MOKE}} = 0$ to the magnetization at 900 Oe. The angular modulations of H_C and R_e were still partly preserved at 400 K, but completely disappeared at 500 and 600 K. We found average values of $H_C(\varphi) \approx 52$ Oe at 400 and 500 K and $H_C(\varphi) \approx 110$ Oe at 600 K. In parallel, the relative remanence decreased for increasing implantation temperature. For the film irradiated at 500 K, a near-rectangular hysteresis loop was observed. This indicates that the displacement of domain walls still exists in the magnetization process. At 600 K, however, this magnetization process had fully disappeared. Similar results were obtained for samples, which were irradiated at 100 K and then annealed for 1 h up to 523 K.

The RBS analyses of these samples performed before and after ion irradiation indicated that, as a consequence of the short heating times, very little thermal diffusion occurred at the Ni/Si interface up to about 500 K. Furthermore, no XRD reflexes due to the possible formation of nickel silicide phases were observed. A much stronger interface broadening due to thermal diffusion was noticed after the 600 K implantation. As usual, we characterize the interface diffusion by the interface variance σ^2, where 2σ denotes the distance between the depths, at which the Ni-concentration changes from 16% to 84% of its bulk value. The increase of the variance due to heating was $\Delta\sigma^2 = 4.6$ nm^2 at 400 K, 38 nm^2 at 500 K, and 88 nm^2 600 K, respectively. Note that the ion-energy was chosen so as to stop the ions within the Ni-films, in order to avoid ion-beam mixing at the interface [22–25].

3.4 External magnetic field during implantation

An important parameter, on which the magnetic texture of the Ni films depends, is the magnetic field at the implantation site during ion irradiation. This was verified by attaching two permanent magnets near the sample, which produce a field of 104 Oe at the center of the implantation spot. For the standard implantation conditions (75 nm Ni/Si(100), 4×10^{14} Xe-ions/cm^2 at 200 keV) the MOKE

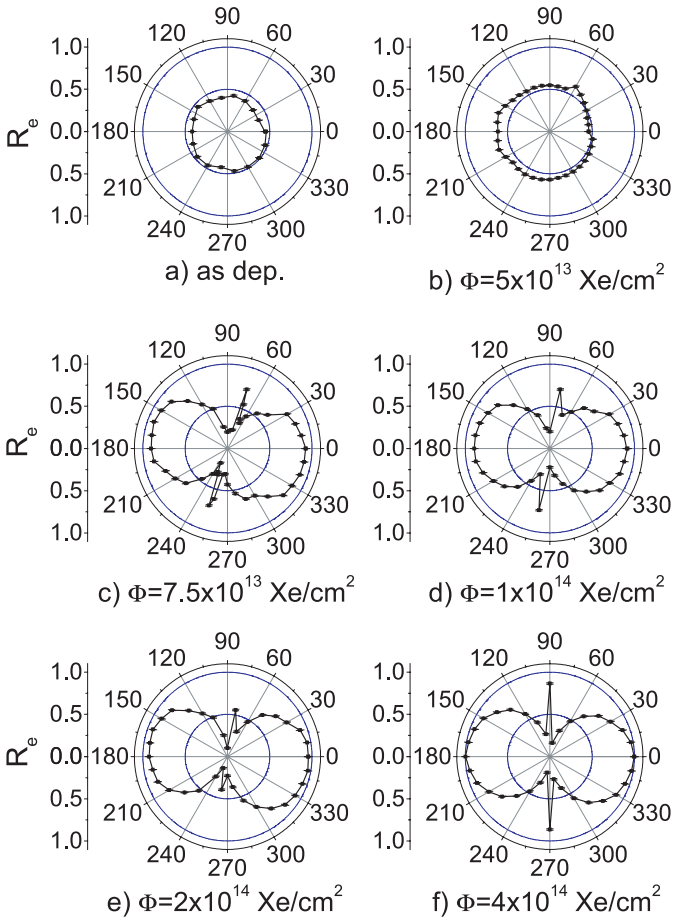

Fig. 7. Fluence dependence of the relative remanence R_e measured at room temperature for 75 nm thick Ni/Si(100)-films irradiated with 200 keV Xe-ions to a fluence of 4×10^{14}/cm^2 at 100 K.

pattern exhibited a magnetic texture, whose symmetry angle φ_0 agreed within 1° with the orientation of the external field. This is illustrated in Figure 6. At this point, it is interesting to note that magnetic fields applied after implantation, as for instance during the MOKE-analyses, did not change the orientation of the magnetic texture, which therefore can be considered to be frozen in. Furthermore, we noted that the alignment of the polarization with the external field was not fulfilled at lower ion fluences (see below).

3.5 Xe-ion fluence dependence

One expects the ion fluence to be among the decisive parameters influencing the magnetic texturing. Therefore, we varied the ion fluence in the range $\Phi = 2.5 \times 10^{13}$–$4 \times 10^{14}$ Xe/cm^2, leaving all other sample and ion parameters constant. This experiment was carried out for flat Ni/Si(100) films under an external polarizing field of 104 Oe in the direction $\varphi = 0$. The resulting polar diagrams of the remanence R_e are displayed in Figure 7 and the fitting parameters R_0 and R_D of equation (1) and

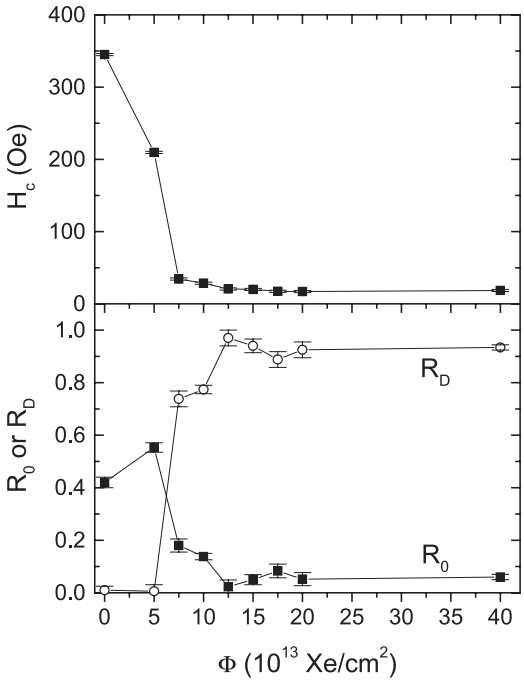

Fig. 8. Fluence dependence of the fitting parameters R_0, R_D and φ_0 (see Eq. (1)) and the coercivity along the easy axis.

the coercivity H_C along the easy axis are summarized in Figure 8.

The data clearly show several stages, in which the magnetic texture evolves. In the as-deposited state and up to about 5×10^{13} Xe-ions/cm^2, there was no magnetic anisotropy in H_C nor in R_e. At the rather modest fluence of 5×10^{13} ions/cm^2, the coercive field H_C dropped from 350 Oe to 210 Oe, but neither H_C nor R_e did show any anisotropy. Above 7×10^{13} Xe-ions/cm^2, the uniaxial anisotropy of H_C and R_e started to develop, with H_C further decreasing to about 35 Oe in its maximum. Above some 2×10^{14} Xe-ions/cm^2, the angular dependence of H_C and R_e reached more or less stable patterns. We also noted that the symmetry angle φ_0 ligned up with the direction of the external field only at the highest fluence of 4×10^{14} Xe-ions/cm^2, but deviated at smaller ion fluences. From the analysis of the XRD data of these samples, we derived a tensile stress of +1.2 GPa after deposition, which decreased for rising ion fluence, becoming zero at 3×10^{14}/cm^2 and slightly compressive (–0.05 GPa) after 4×10^{14} ions/cm^2 were implanted into the specimen.

3.6 Xe-ion energy dependence

In the context of inverse magnetostriction, one has to distinguish three types of strains or stresses in the Ni-films: internal stresses produced during deposition of the films onto the substrates, internal stresses induced by the implanted, non-soluble noble-gas ions or their radiation defects, and external stress exerted during handling or mounting the samples. Our previous PAC- and MOKE-analyses of ion-irradiated Ni-films [13,14] had not taken

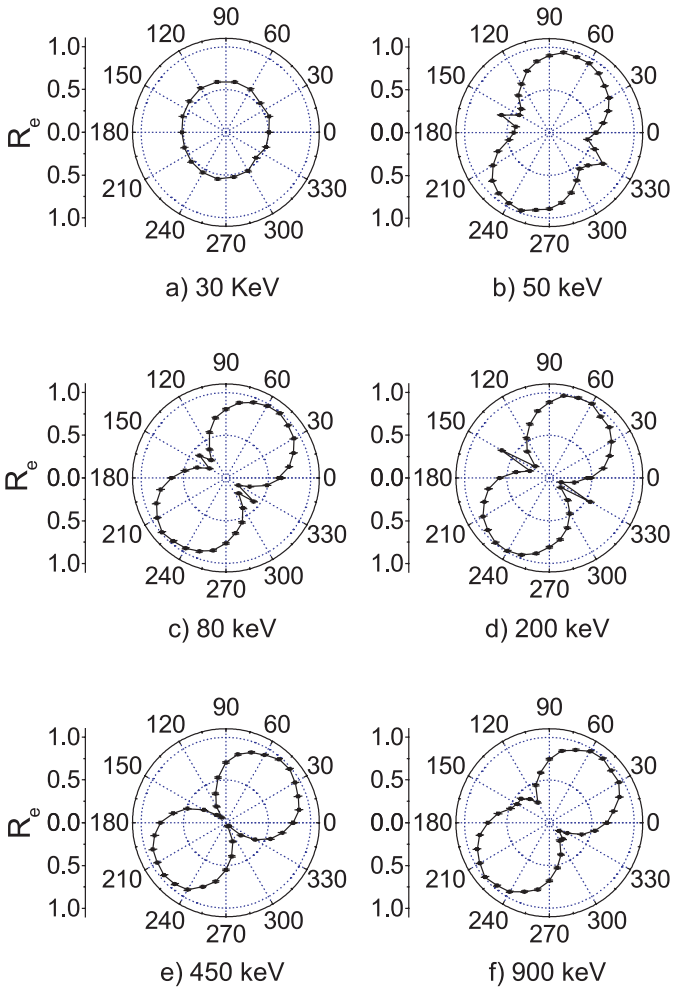

Fig. 9. Angular modulations of the relative remanence, R_e, in 75 nm thick Ni/SiO_2-films, irradiated with 4×10^{14} Xe-ions/cm^2 at the ion energies given.

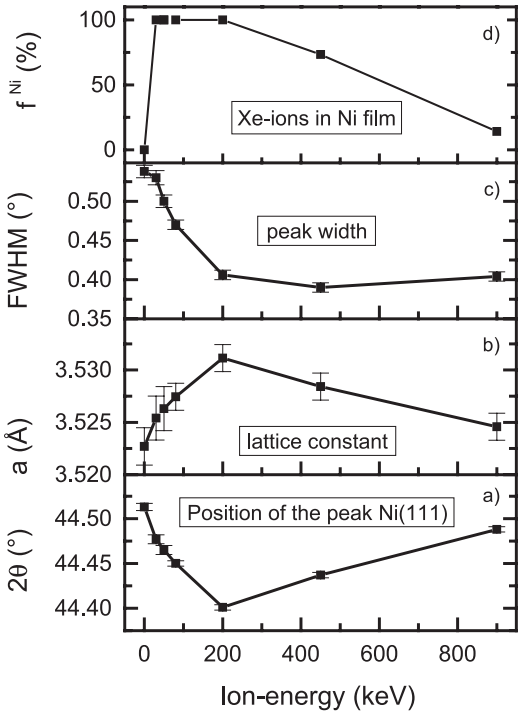

Fig. 10. XRD-analyses of Xe-irradiated 75 nm Ni-films as function of the ion energy: (a) Position of the Ni(111)-peak; (b) Lattice constant as calculated from the Ni(111)-peak; (c) Full-width at half-maximum of the Ni(111)-peak; (d) Fraction of the Xe-ions stopped in the Ni-films.

particular care concerning the stress conditions in the samples. For good thermal contact, these samples had been tightly clamped by two or four screws to the copper target holder, which was connected to the liquid nitrogen dewar. This type of fixing may have caused external (and unknown) stress in the films. In the present study, the samples were fixed carefully with silver paste on the substrates. Furthermore, the effects of ion-induced internal stress were investigated by variation of the ion energy. By bending and relaxing the samples to well defined curvatures, the effects of external stress were studied separately (see Sect. 3.7).

By varying the Xe-ion energy between 30 and 900 keV we changed the ion-induced internal stress, which arises from different fractions of gas ions stored in the Ni-film (or the substrate) and different densities of radiation damages due to nuclear stopping. Both effects possibly lead to different lattice dilations in the Ni-film. In this series of measurements, we used 10×7 mm^2, 75 nm thick Ni films deposited on a-SiO_2 substrates and irradiated with 4×10^{14} Xe-ions/cm^2 at 200 keV. SiO_2 substrates were chosen in order to minimize ion-induced mixing and Ni-silicide formation at the interface [22–26].

The corresponding polar MOKE-diagrams of the remanence R_e are displayed in Figure 9. At 30 keV, the magnetic anisotropy was negligible, but started developing at 50 keV and was most pronounced at 200 and 450 keV. Fitting the data again with the expression (1), the parameters varied strongly up to 50 keV Xe-energy, but little at higher energies: $R_0 = 0.02 - 0.06$, $R_D = 0.93 - 0.96$.

Figure 10 summarizes the microstructural information obtained from XRD, i.e. the position of the Ni(111)-peak (Fig. 10a), the deduced lattice constant a (Fig. 10b) and peak width (Fig. 10c), and the relative fraction of xenon sticking in the Ni-film (Fig. 10d). Up to 200 keV, all ions were deposited in the Ni-film, while at 450 and 900 keV, this fraction dropped to 75% and 15%, respectively, as predicted from SRIM2000 computer simulations [33] and verified by the RBS analyses. As shown in Figure 10b, the average Ni-lattice constant increased from $a = 0.35227$ nm at 30 keV ion energy to $a = 0.35311$ nm at 200 keV and then dropped to $a = 0.35246$ nm at 900 keV, close to the value of bulk Ni, $a = 0.35238$ nm. The full width at half maximum (FWHM) of the (111) reflex dropped from 0.54° at 30 keV to 0.40° at 200 keV and then stayed at this value at 450 and 900 keV (Fig. 10c). Selecting the ion energy in such a fashion that its distribution covers the full film thickness therefore produced the highest average lattice dilation and strongest magnetic anisotropy, while collecting the ions near the surface (30 keV) or mainly in

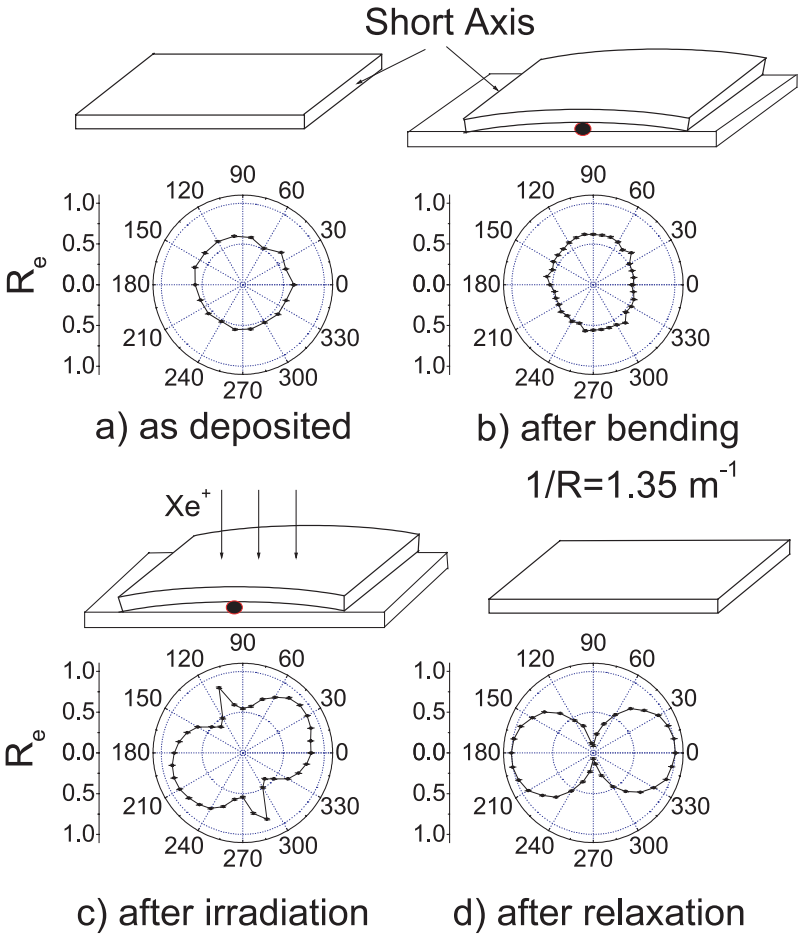

Fig. 11. Polar diagrams of the remanence R_e measured during a cycle of sample deposition, bending, irradiation and relaxation. The data refer to a 75 nm Ni/Si(100)-film irradiated with 4×10^{14} Xe-ions/cm^2 at 200 keV. The curvature was $1/R = 1.35$ m^{-1}.

the substrate (900 keV) induced little lattice distortion in the Ni-film and a weaker magnetic texture.

3.7 Experiments with bent samples

The variation of external stress during or after ion implantation was studied for 75 nm Ni/Si(100) samples, 10×7 mm^2 in size, deposited in the center of 40×15 mm^2 Si(100)-wafers, which were bent along the long or short axis. A typical treatment cycle and the corresponding polar diagrams of the remanence R_e are illustrated in Figure 11. The as-deposited, flat sample did not show any preferred in-plane magnetization (a). After bending to a curvature of $1/R = 1.35$ m^{-1}, the in-plane magnetization was still nearly isotropic (b). If now the sample was irradiated with 4×10^{14} Xe-ions/cm^2, a magnetic texture appeared (c), which was even more pronounced after the sample was relaxed to its original flat shape (d). The relaxation induced a strong compressive stress, which was oriented perpendicular to the bending axis. Due to inverse magnetostriction and the large negative magnetostriction coefficient of Ni, this stress led to a pronounced magnetic texture pointing perpendicular to the bending axis, i.e. $\varphi_0 = 0°$. This cycle of measurements was repeated for various curvatures $1/R \leq 1.96$ m^{-1} and for the bending axis chosen either along the short or the long axis. As shown in Figure 12, the symmetry angle φ_0 increased with the curvature and saturated at $\varphi_0 = 90°$ for large curvatures. In Figure 13, the deduced symmetry angles φ_0 obtained for both bending axes are plotted versus the curvature $1/R$.

4 Discussion

The MOKE- and VSM-measurements presented in Section 3 show that already rather small fluences of heavy ions induce a uniaxial magnetization and a strong decrease of the coercivity upon implantation into polycrystalline Ni-films of tens of nm thickness. This magnetic texture is thermally stable up to implantation and/or annealing temperatures of about 400 K and is most pronounced if the implanted ions are distributed over the full film thickness with the ion range located near the middle of the films. The type and crystallinity of the substrate do not appear to have any influence on the magnetization, while an external magnetic field of some 100 Oe during the implantation and/or ion-induced or external stress during

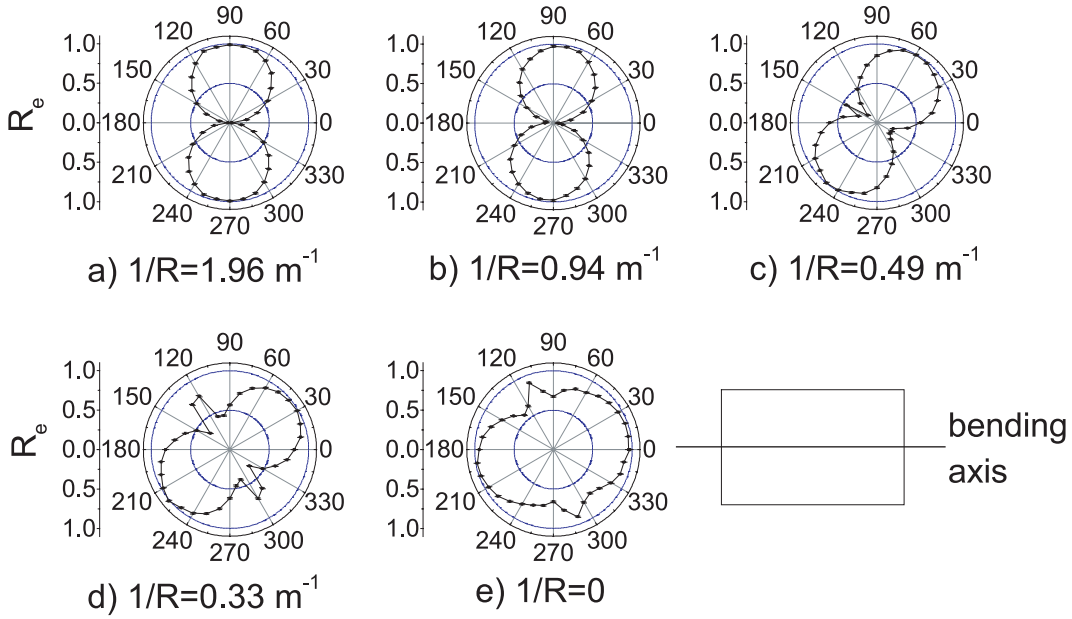

Fig. 12. Curvature dependence of the relative remanence $R_e(\varphi)$. The films were bent to a curvature of $1/R \leq 1.96$ m^{-1}, then irradiated with 4×10^{14} Xe-ions/cm^2 and finally relaxed before carrying out the MOKE-analyses. The bending axis is indicated. Note that the rotation of the symmetry axis φ_0 increases with the curvature.

or after the implantation determine the orientation of this texture.

These findings corroborate previous results in ion-irradiated polycrystalline Ni-films or Ni-bulk material obtained with perturbed angular correlation spectroscopy for implanted ^{111}In tracers [12,34]. Similar results have also been obtained with Mössbauer spectroscopy for polycrystalline, ion-irradiated Fe-films [15,19,29,35]. These hyperfine data demonstrate that magnetic texturing generally implies two steps, firstly the switching of the initially often isotropic magnetization into the film plane and secondly its orientation within the film plane. We also mention here the observation of pronounced magnetic texturing effects in polycristalline CoFe (permendur) films upon Xe-ion irradiation [36].

If we neglect the sharp peaks along the hard axis occasionally seen at higher fluences (see Fig. 3), the polar diagrams of the relative remanence R_e can be parametrized with the expression given in equation (1), valid for stripe domain structure. Here R_D represents the sum of the magnetic moments within the domains parallel to the direction φ_0, while R_0 denotes the isotropic component. (Our preliminary Magnetic Force Microscopy scans indeed demonstrated a parallel domain structure with a typical period of 0.2 μm in the as-deposited Ni films and of about 2 μm after Xe-irradiation.)

The following discussion aims at giving a scenario of the magnetic texturing effect and to estimate the influence of some of the parameters on the remanence R_D/R_0 and coercivity H_C. We first discuss the influence of the external stress on the symmetry angle φ_0 of the easy axis. The orientation φ_0 of the uniaxial anisotropy is determined by

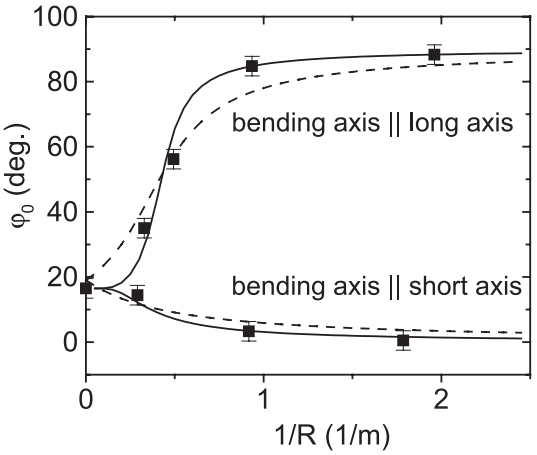

Fig. 13. Curvature dependence of the easy-axis angle φ_0. The fit corresponds to the expression (5), where the relationship between $1/R$ and σ as given by either equation (6) (solid line) or (7) (dashed line) was used.

the interplay of the anisotropy energy density,

$$E_u = K_u \sin^2(\varphi - \varphi_0), \tag{2}$$

K_u being the anisotropy constant, and the stress-induced energy density,

$$E_s = -(3/2)\lambda\sigma\cos^2\varphi, \tag{3}$$

where λ denotes the magnetostriction constant ($\lambda = -3.3 \times 10^{-5}$ for polycrystalline Ni) and σ the stress. By setting

$$\partial(E_u + E_s)/\partial\varphi = 0 \quad \text{for} \quad \varphi = \varphi_0, \tag{4}$$

one arrives at the condition [37]

$$\tan 2\varphi_0 = \sin 2\varphi_0/[\cos 2\varphi_0 + (3/2)\lambda\sigma/K_u]. \quad (5)$$

Assuming that the stress σ is proportional to the curvature $1/R$ for large values of $1/R$ and goes to zero for flat samples, we parametrized $\sigma(R)$ as

$$\sigma(R) = \sigma_\infty/(e^{R/b} - 1) \rightarrow \sigma_\infty\, b/R \ \text{ for } \ R \rightarrow 0. \quad (6)$$

The fit to the measured function $\varphi_0(1/R)$ shown in Figure 12 gave the parameters $\sigma_\infty = \lambda\sigma/K_u = -3.3(5)$ and $b = 1.3(1)$ m.

As a second parametrization we used the Stoney equation [38],

$$\sigma(R) = [Y t_s^2/6t_f^2](1/R - 1/R_0), \quad (7)$$

where t_f and t_s are the film and substrate layer thicknesses, Y the biaxial modulus, and $1/R$ and $1/R_0$ the sample curvatures before and after bending. This fit of the function $\varphi_0(1/R)$, which is also illustrated in Figure 13, is still acceptable, but follows the data not as closely as equation (6). The probable reason is that for small external stress (large bending radii) the effects of internal stress due to sample deposition and/or Xe-implantation are relatively more important and lead to deviations from the Stoney equation.

As noted before, the texturing effect is most pronounced, if the ions are stored in the middle of the Ni films, while little texturing arises, if the ion range is much less than the film thickness (see Fig. 9). Furthermore, the anisotropy remains, although with smaller amplitude, if the ions penetrate the Ni-films and come to rest in the substrate. (This latter aspect was confirmed in a recent experiment [39], in which a 75 nm Ni-film on Si(100) was irradiated with a 350 MeV Au-beam, whose range in the substrate was some 25 μm [39]. Even in this case a small texturing effect was observed.) We interpret these findings that it is not the storage of the implanted ions themselves, which mainly causes the magnetic texturing, but rather the radiation damage produced by them. It is known that the defect yield of extended radiation defects, such as vacancy clusters, at room temperature, where the MOKE-analyses were carried out, is of the order of 0.1–0.2 in fcc-nickel and copper, but only about 10^{-3} in bcc-Fe [40]. At room temperature, most point defects (interstitials, single or double vacancies) have annealed out.

Müller et al. [15,29,35,41] very recently studied magnetic texturing of ion-irradiated poly- and single-crystalline iron films, 50–75 nm thick and prepared by either electron evaporation on Si(100) or pulsed-laser deposition on MgO substrates. These investigations revealed some important clues for interpreting the present results in nickel. While the Xe irradiation of the epitaxial Fe layer on MgO did not induce any change of the magnetic anisotropy [41], irradiations of the polycrystalline Fe-layers with Ne, Fe, Kr or Xe ions resulted in pronounced anisotropies similar to those observed in the present Ni films [15,35]. In the case of Xe ions impinging on Fe, the ion fluence to achieve a full anisotropy was roughly one order of magnitude higher than in the case of Xe on Ni, which is consistent with the fact that the density of extended defects in Fe is roughly by the same factor smaller than in Ni [40]. Furthermore, in the polycrystalline samples, the Mössbauer spectra indicated large fractions of hyperfine fields consistent with extended defects and a highly disturbed lattice, contrary to the single-crystalline Fe sample, in which the hyperfine field indicated mainly substitutional defect-free lattice sites. Finally, the XRD analysis of the polycrystalline Fe-samples revealed a high tensile stress of +3.8 GPa after deposition, which, for rather small fluences of all ions, was released in favor of a small compressive stress of –1.5 GPa [29].

In analogy with the directional order model for alloys [42], a magnetic anisotropy can be explained by the alignment of defects or anisotropic vacancy clusters in the grain boundaries [43]. On the basis of electron micrographs of polycrystalline, 30 nm thin iron films, Antonov et al. [44] proposed a mechanism for the induced magnetic anisotropy by considering the role of vacancy clusters with ellipsoidal shapes. These authors estimated the anisotropy for various concentrations, distributions, eccentricities and orientations of voids, and obtained values of the anisotropy constant K_u of up to 2×10^5 erg/cm^3. In particular, the formation of dislocations and dislocation loops [40,43] by noble-gas or self-ion irradiation seems to play an important role and strongly depends on the irradiated material, its crystallographic structure, the projectile mass and the characteristics of the damage cascade. While in the fcc-metals nickel or copper films extended defects were found for ion fluences exceeding 10^{14} ions/cm^2, comparable defect densities were observed in bcc-iron only at much higher fluences.

Obviously, a detailed knowledge of the microstructural changes induced by the ion irradiation is required to test whether the approach of Antonov et al. may explain the present findings. The XRD data presented in Figure 10 indicate the largest lattice expansion, if the ions are stored in the middle of the Ni-film; at 4×10^{14} Xe-ions/cm^2, the lattice constant increased by 65(15) pm. It has been argued that both the implanted insoluble noble-gas ions and the extended defects created during their implantation are responsible for the magnetostriction, which in turn trigger the magnetic texturing. Evidently, transmission electron microscopy is required to picture the changes of the defect structure and to try to determine the size and orientation of the extended defects. TEM may also give access to clarify the orientation of the anisotropy in the case that no external magnetic nor stress field are available during the implantation.

The parameter most sensitive to changes of the magnetization is the coercivity H_C, which is known to depend strongly on the defect and grain structure and on the internal strains of the specimen [45]. In addition, impurities incorporated either during deposition or ion implantation can play a dominant role in explaining large values of H_C. Thus, the high coercivity of the Ni-films after electron-gun deposition and its strong reduction during the irradiation can be explained by the reduction in the intrinsic stress.

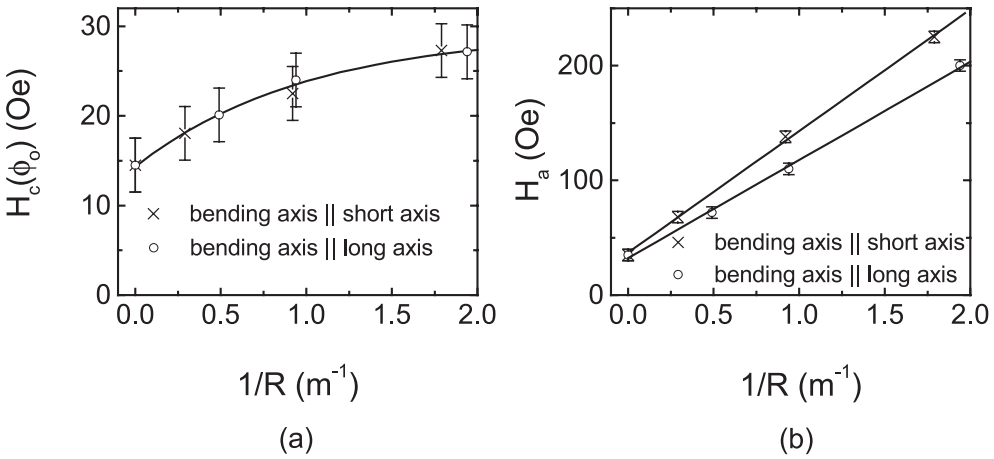

Fig. 14. Coercive field $H_C(\varphi_0)$ of the easy axis (a) and the anisotropy field H_k measured along the hard axis (b), plotted versus the curvature $1/R$.

The MOKE magnetization curves gave also information on how the coercive field along the easy axis, $H_C(\varphi_0)$, and the anisotropy field along the hard axis, H_a, depend on the external stress. As shown in Figure 14a, $H_C(\varphi_0)$ increased smoothly from $H_C(\varphi_0) = 14(3)$ Oe at $1/R = 0$ to $H_C(\varphi_0) = 27(3)$ Oe for $1/R = 2.0$ m^{-1}, where it appears to reach saturation. For both bending directions, H_a varied linearly (and with very similar slopes) with the curvature $1/R$ (see Fig. 14b).

5 Conclusions

We have demonstrated that polycrystalline Ni-films, tens of nm thick and rectangular in shape, develop a uniaxial strain-induced anisotropy if irradiated with Xe-ions at rather low fluences of some 10^{13} ions/cm^2. This magnetic texture is most pronounced if the ion range matches half the film thickness. It neither appears to depend on the substrate nor on the size of the ion beam spot and is thermally stable up to about 400 K. An external magnetic field during implantation and/or a well defined stress field are decisive parameters, which govern the orientation of the magnetic texture. Inverse magnetostriction, either due to the internal strain produced by the extended radiation defects and/or the implanted insoluble noble-gas ions or by external stress when bending the samples, is suggested to be mainly responsible for the effect [6,8]. Qualitatively similar results, but of very different magnitude and origin have recently been obtained in heavy-ion-irradiated Fe, Co, permalloy and permendur films of similar thickness [15–19,35,36,41,46]. Despite these comprehensive studies we have so far not been able to account for the orientation of the MOKE pattern in the absence of any external stress or magnetic field.

It is a pleasure to thank Detlef Purschke and Andreas König for their help during the ion irradiations and Sankar Dhar and Ettore Carpene for performing some of the RBS- and XRD-analyses. We are indebted to Michael Farle (Universität Duisburg), Wolfgang Felsch and Konrad Samwer (Universität Göttingen), Ulrich Gradmann (TU Clausthal), Jürgen Kirschner and Dirk Sander (MPI Halle) for various suggestions and discussions. This work has been supported by Deutsche Forschungsgemeinschaft, Bonn.

References

1. B. Heinrich, J.A.C. Bland, in *Ultrathin Magnetic Structures* (Springer, Berlin, 1994), p. 21
2. A. Huber, R. Schäfer, *Magnetic Domains – the Analysis of Magnetic Microstructures* (Springer, Berlin, 1998)
3. A.A. Hirsch, A. Ahilea, N. Friedman, Phys. Lett. A **28**, 763 (1969)
4. M. Takahashi, D. Watanabe, T. Kono, S. Ogawa, J. Phys. Soc. Jpn **15**, 1351 (1961)
5. K. Itoh, J. Magn. Magn. Mater. **95**, 237 (1991)
6. W.A. Lewis, M. Farle, B.M. Clermens, R.C. White, J. Appl. Phys. **75**, 5644 (1994)
7. D. Garcia, J.L. Munoz, F.J. Castano, C. Prados, A. Asenjo, J.M. Garcia, M. Vazquez, J. Appl. Phys. **85**, 4809 (1999)
8. M. Farle, H. Saffari, W.A. Lewis, E. Kay, S.B. Hagstrom, IEEE Trans. Magn. MAG **28**, 2940 (1992)
9. C. Chappert, H. Bernas, J. Ferré, V. Kottler, J.-P. Jamet, Y. Chen, E. Cambril, T. Devolder, F. Rousseaux, V. Mathet, H. Launois, Science **280**, 1919 (1998)
10. H. Bernas et al., Nucl. Instr. Meth. B **148**, 872 (1999)
11. T. Aign, P. Meyer, S. Lemerle, J.P. Janet, J. Ferré, V. Mathet, C. Chappert, J. Gierak, C. Vieu, F. Rousseaux, H. Launois, H. Bernas, Phys. Rev. Lett. **81**, 5656 (1998)
12. P. Wodniecki, T. Corts, K.P. Lieb, M. Uhrmacher, Nucl. Instr. Meth. B **62**, 394 (1992)
13. M. Neubauer, N. Reinecke, M. Uhrmacher, K.P. Lieb, M. Münzenberg, W. Felsch, Nucl. Instr. Meth. B **139**, 332 (1998)
14. M. Neubauer, K.P. Lieb, P. Schaaf, M. Uhrmacher, Phys. Rev. B **53**, 10237 (1996)
15. G.A. Müller, R. Gupta, K.P. Lieb, P. Schaaf, Appl. Phys. Lett. **82**, 73 (2003)
16. K. Zhang, R. Gupta, K.P. Lieb, Y. Luo, G.A. Müller, P. Schaaf, M. Uhrmacher, Europhys. Lett. **64**, 668 (2003)

17. K. Zhang, R. Gupta, K.P. Lieb, Y. Luo, G.A. Müller, P. Schaaf, M. Uhrmacher, J. Magn. Magn. Mater. **272-276**, 1162 (2004)
18. K. Zhang, R. Gupta, G.A. Müller, P. Schaaf, K.P. Lieb, Appl. Phys. Lett. **84**, 3915 (2004)
19. K.P. Lieb, K. Zhang, G.A. Müller, P. Schaaf, M. Uhrmacher, W. Felsch, M. Münzenberg, Acta Phys. Polon. A **100**, 751 (2001)
20. K. Zhang, K.P. Lieb, P. Schaaf, M. Uhrmacher, W. Felsch, M. Münzenberg, Nucl. Instr. Meth. B **161-163**, 1016 (2000)
21. M. Uhrmacher, K. Pampus, F.J. Bergmeister, D. Purschke, K.P. Lieb, Nucl. Instr. Meth. B **9**, 234 (1985)
22. K.N. Tu, W.K. Chu, J.W. Mayer, Thin Solid Films **25**, 403 (1975)
23. D.M. Scott, M.-A. Nicolet, Nucl. Instr. Meth. **182/183**, 655 (1981)
24. L.R. Zhang, L.S. Hung, J.W. Mayer, Appl. Phys. Lett. **41**, 646 (1982)
25. S. Dhar, P. Schaaf, N. Bibic M. Milosavljevic, E. Hooker, K.P. Lieb, Appl. Phys. A **73**, 773 (2003)
26. M. Schwickert, K.P. Lieb, W. Bolse, M. Gustafsson, J. Keinonen, Nucl. Instr. Meth. B **147**, 238 (1999); K.P. Lieb, M. Schwickert, W. Bolse, M. Gustafsson, J. Jokinen, J. Keinonen, Nucl. Instr. Meth. B **148**, 951 (1999)
27. R.M.A. Azzam, *Ellipsometry and Polarized Light* (North Holland, Amsterdam, 1977)
28. M. Münzenberg, diploma thesis, Göttingen (1997) unpublished
29. G.A. Müller, doctoral thesis, Göttingen (2003)
30. S. Chikazumi, *Physics of Ferromagnetism* (Clarendon Press, Oxford, 1997), p. 450. S
31. A.H. Morrish, *The Physical Principles of Magnetism* (Wiley and Sons, New York, 1991)
32. M. Hanson, C. Johansson, E.B. Svedberg, J. Magn. Magn. Mater. **236**, 139 (2001)
33. Program SRIM2000, J.F. Ziegler, J.P. Biersack, U. Littmark, *The Stopping and Range of Ions in Solids* (Pergamon Press, NY, 1999)
34. A. Kulinska, K.P. Lieb, G.A. Müller, M. Uhrmacher, K. Zhang, J. Magn. Magn. Mater. **272-276**, 1149 (2004)
35. G.A. Müller, A. Kulinska, K. Zhang, R. Gupta, P. Schaaf, M. Uhrmacher, K.P. Lieb, Hyp. Int. **151/152**, 223 (2003)
36. R. Gupta, G.A. Müller, P. Schaaf, K. Zhang, K.P. Lieb, Nucl. Instr. Meth. B **216**, 350 (2004)
37. A.H. Morrison, *The Physical Principles of Magnetism* (Wiley and Sons, New York, 1965), p. 400
38. G.G. Stoney, Proc. Royal Soc. (London) A **82**, 172 (1909)
39. K.P. Lieb, privote communication
40. M.L. Jenkins, M.A. Kirk, W.J. Phythian, J. Nucl. Mat. **205**, 16 (1993)
41. G.A. Müller, K.P. Lieb, E. Carpene, K. Zhang, P. Schaaf, J. Faupel, H.U. Krebs, Hyp. Int. (in press)
42. S. Chikazumi, Phys. Rev. **85**, 918 (1955)
43. A.G. Lesnik, Phys. Stat. Sol. **35**, 959 (1969); A.G. Lesnik, A.I. Mitsek, V.N. Pushkar, Phys. Stat. Sol. (a) **17**, 697 (1973)
44. L.I. Antonov, V.V. Veter, L.A. Yudina, G.V. Kozodoy, E.L. Fedorova, V.V. Yudin, Fiz. metal. metalloved. **43**, 518 (1977)
45. E. Kneller, *Ferromagnetismus* (Springer-Verlag, Berlin, Göttingen, Heidelberg, 1962)
46. R. Gupta, K.P. Lieb, Y. Luo, G.A. Müller, P. Schaaf, M. Uhrmacher, K. Zhang, submitted to J. Appl. Phys.